

## Single-particle properties of a strongly interacting Bose-Fermi mixture with mass and population imbalance

Koki Manabe,<sup>1</sup> Daisuke Inotani,<sup>2</sup> and Yoji Ohashi <sup>1</sup>

<sup>1</sup>*Department of Physics, Keio University, 3-14-1 Hiyoshi, Kohoku-ku, Yokohama 223-8522, Japan*

<sup>2</sup>*Research and Education Center for Natural Sciences, Keio University, 4-1-1 Hiyoshi, Kohoku-ku, Yokohama 223-8521, Japan*



(Received 29 July 2019; published 5 December 2019)

We theoretically investigate strong-coupling properties of a Bose-Fermi mixture. In the mass- and population-balanced case, two of the authors have shown that a strong heteropairing interaction in this mixture brings about coupling phenomena between Fermi atomic excitations and Bose atomic and composite molecular excitations, that appear as an anomalous multiple peak structure in the single-particle spectral weight (SW) [Kharga, Inotani, Hanai, and Ohashi, *J. Phys. Soc. Jpn.* **86**, 084301 (2017)]. In this paper, we show that, although these many-body phenomena are sensitive to mass and population imbalances between the Bose and Fermi components, SW still exhibits the multiple peak structure in moderately mass-imbalanced  $^{87}\text{Rb}$ - $^{40}\text{K}$  and  $^{23}\text{Na}$ - $^{40}\text{K}$  mixtures. We also point out that the photoemission spectrum is a useful quantity to observe this spectral anomaly. Since a real trapped Bose-Fermi mixture is usually accompanied by mass and (local) population imbalances, our results would contribute to the study of a strongly interacting Bose-Fermi mixture, under realistic imbalanced conditions.

DOI: [10.1103/PhysRevA.100.063609](https://doi.org/10.1103/PhysRevA.100.063609)

### I. INTRODUCTION

The high tunability of an ultracold atomic gas has contributed to the development of quantum many-body physics discussed in various research fields [1–4]: Using an optical lattice technique, Greiner and coworkers have observed the superfluid–Mott-insulator transition in a  $^{87}\text{Rb}$  Bose gas [5]. In  $^{40}\text{K}$  [6] and  $^6\text{Li}$  Fermi gases [7–9], the superfluid phase transition and the BCS-BEC crossover phenomenon [10–14] have been realized, by using a tunable pairing interaction associated with a Feshbach resonance [15].

Besides Bose gas and Fermi gas, a gas mixture of Bose and Fermi atoms has also extensively been studied in cold atom physics, both experimentally [16–21] and theoretically [22–27]. This Bose-Fermi mixture is similar to a  $^4\text{He}$ - $^3\text{He}$  mixture, as well as quark matter in high-energy physics [28]. Using this similarity, as well as the advantage that one can tune the strength of a Bose-Fermi pairing interaction by using a heteronuclear Feshbach resonance, Ref. [28] suggests that this atomic mixture may be used as a quantum simulator for the study of dense QCD matter, where a bound di-quark (boson) and an unpaired quark (fermion) form a nucleon (composite fermion).

For a mass- and population-balanced Bose-Fermi mixture, two of the authors have recently shown that a strong Bose-Fermi pairing interaction causes couplings between Bose atomic excitations and Fermi atomic excitations (Bose-Fermi coupling), as well as atomic excitations and molecular excitations (atom-molecule coupling) [26]. As an interesting phenomenon associated with these couplings, the Fermi component of the single-particle spectral weight (SW) has been known to exhibit a triple-peak structure, consisting of two sharp peaks along the free fermion dispersion and composite

molecular dispersion, and a broad downward peak related to Bose single-particle excitations. Here, we recall that SW in a free Fermi gas only has a single peak line along the free particle dispersion. In a two-component Fermi gas in the BCS-BEC crossover region, SW is known to exhibit a double-peak structure associated with the pseudogap phenomenon originating from strong-pairing fluctuations [29–32]. Thus, the triple-peak structure in the Fermi SW is expected to be characteristic of a strongly interacting Bose-Fermi mixture.

To confirm this expectation, however, one should remember that any real Bose-Fermi mixture is composed of different kinds of atoms or different isotopes, such as  $^{87}\text{Rb}$ - $^{40}\text{K}$  [16–18] and  $^{23}\text{Na}$ - $^{40}\text{K}$  [19,20] gases, so that it is always accompanied by mass imbalance. In addition, when it is trapped in a harmonic potential, bosons and fermions have different density profiles. Thus local population imbalance is unavoidable, even when both components have the same number of atoms. Although a box-type trap has recently been invented [33–35] (where a trapped gas is almost uniform), the conventional harmonic trap is still used in many experiments. At this stage, it is unclear to what extent these realistic situations affect the above-mentioned many-body coupling phenomena obtained in the somehow academic mass- and population-balanced case. We briefly note that a highly population-imbalanced Bose-Fermi mixture has recently attracted much attention in the study of the Bose polaron [36–38].

In this paper, we investigate single-particle properties of a Bose-Fermi mixture with a heteronuclear Feshbach resonance. Extending the previous work [26] to include mass and population imbalances, we examine how these affect strong-coupling corrections to SW. We clarify whether or not the many-body coupling phenomena obtained in the mass- and population-balanced case survive in mass-imbalanced

$^{87}\text{Rb}$ - $^{40}\text{K}$  and  $^{23}\text{Na}$ - $^{40}\text{K}$  mixtures. As an observable quantity related to SW, we also deal with the photoemission spectrum [39–43].

This paper is organized as follows. In Sec. II, we explain our formulation. We separately examine effects of population imbalance and mass imbalance in Secs. III, and IV, respectively. In Sec. V, we pick up a  $^{87}\text{Rb}$ - $^{40}\text{K}$  mixture as well as a  $^{23}\text{Na}$ - $^{40}\text{K}$  mixture as two typical examples of mass-imbalanced Bose-Fermi mixtures. Throughout this paper, we set  $\hbar = k_B = 1$ , and the system volume  $V$  is taken to be unity, for simplicity.

## II. FORMULATION

We consider a gas mixture of single-component Bose atoms and single-component Fermi atoms, with a heteronuclear Feshbach resonance. This Bose-Fermi mixture is modeled by the Hamiltonian

$$H = \sum_{p,s=B,F} \xi_p^s c_{p,s}^\dagger c_{p,s} - U_{\text{BF}} \sum_{p,p',q} c_{p+q,B}^\dagger c_{p'-q,F} c_{p',F} c_{p,B}, \quad (1)$$

where  $c_{p,s}^\dagger$  is the creation operator of a Bose ( $s=B$ ) and a Fermi ( $s=F$ ) atom.  $\xi_p^s = \varepsilon_p^s - \mu_s = p^2/(2m_s) - \mu_s$  is the kinetic energy of the  $s$  component, measured from the chemical potential  $\mu_s$  (where  $m_s$  is an atomic mass).  $-U_{\text{BF}} (< 0)$  is a Bose-Fermi pairing interaction, which is assumed to be tunable by a heteronuclear Feshbach resonance. This contact-type interaction brings about the ultraviolet divergence. As usual, we absorb this singularity into the  $s$ -wave scattering length  $a_{\text{BF}}$  [25], which is related to the bare pairing interaction  $-U_{\text{BF}}$  as

$$\frac{4\pi a_{\text{BF}}}{m} = -\frac{U_{\text{BF}}}{1 - U_{\text{BF}} \sum_p^{p_c} \frac{m}{p^2}}. \quad (2)$$

Here,  $m = 2m_B m_F / (m_B + m_F)$  is twice the reduced mass, and  $p_c$  is a cutoff momentum.

We measure the interaction strength in terms of  $(k_{\text{tot}} a_{\text{BF}})^{-1}$  [25], where  $k_{\text{tot}} = (3\pi^2 N_{\text{tot}})^{1/3}$  with  $N_{\text{tot}} = N_B + N_F$  being the total number of atoms (where  $N_{s=B,F}$  is the number of atoms in the  $s$  component). In the population-balanced case ( $N_B = N_F$ , or  $N_{\text{tot}} = 2N_F$ ), this scaled variable  $k_{\text{tot}}$  coincides with the Fermi momentum  $k_F = (6\pi^2 N_F)^{1/3}$  of a single-component Fermi gas with  $N_F$  atoms. This simple relation is no longer satisfied when  $N_B \neq N_F$ . However, even in such a case, apart from the numerical constant with  $O(1)$ ,  $k_{\text{tot}}^{-1}$  physically means the interparticle spacing ( $\sim N_{\text{tot}}^{-1/3}$ ).

In this paper, we only deal with a uniform gas, ignoring effects of a harmonic trap. However, the local population imbalance coming from the difference of the density profile between the Bose and Fermi components in a trap is partially examined by considering the population-imbalanced case ( $N_B \neq N_F$ ).

Strong-coupling corrections to Bose and Fermi single-particle excitations can be described by the self-energy  $\Sigma_{s=B,F}(\mathbf{p}, i\omega_s)$  in the single-particle thermal Green's functions,

$$G_{s=B,F}(\mathbf{p}, i\omega_s) = \frac{1}{i\omega_s - \xi_p^s - \Sigma_s(\mathbf{p}, i\omega_s)}, \quad (3)$$

where  $i\omega_B$  ( $i\omega_F$ ) is the boson (fermion) Matsubara frequency.

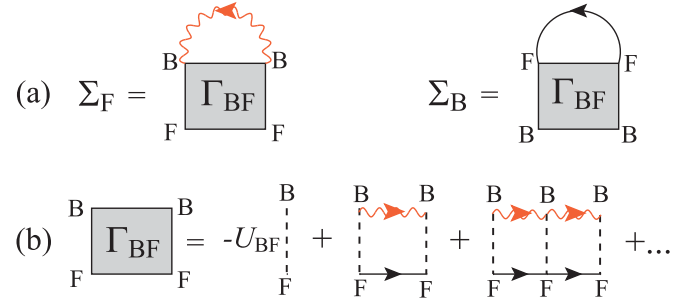


FIG. 1. (a) Self-energies  $\Sigma_{s=B,F}$  in iTMA. (b) Bose-Fermi scattering matrix  $\Gamma_{\text{BF}}(\mathbf{q}, i\omega_F)$  in Eq. (10), physically describing heteropairing fluctuations. The solid line is the bare Fermi Green's function  $G_F^0$  in Eq. (7). The wavy line is the *modified* Bose Green's function  $\tilde{G}_B^0$  in Eq. (5). The dashed line is the heteropairing interaction  $-U_{\text{BF}}$ .

We evaluate  $\Sigma_s(\mathbf{p}, i\omega_s)$  within the framework of the  $T$ -matrix-type approximation developed in Ref. [26]. This approximation is diagrammatically described in Fig. 1. This diagrammatic structure is formally the same as that in the ordinary (non-self-consistent)  $T$ -matrix approximation (TMA) [25,44,45]; however, the crucial difference is that the bare Bose Green's function,

$$G_B^0(\mathbf{p}, i\omega_B) = \frac{1}{i\omega_B - \xi_p^B}, \quad (4)$$

used in the TMA self-energy is now replaced by the *modified* one [26]:

$$\tilde{G}_B^0(\mathbf{p}, i\omega_B) = \frac{1}{i\omega_B - \tilde{\xi}_p^B}. \quad (5)$$

Here,  $\tilde{\xi}_p^B = \xi_p^B + \Sigma_B(\mathbf{0}, 0) \equiv \varepsilon_p^B - \tilde{\mu}_B$  [where  $\tilde{\mu}_B = \mu_B - \Sigma_B(\mathbf{0}, 0)$ ] involves the self-energy correction at  $\mathbf{p} = i\omega_B = 0$ . The modified Green's function  $\tilde{G}_B^0(\mathbf{p}, i\omega_B)$  in Eq. (5) then satisfies the Hugenholtz-Pines theorem [46],

$$\mu_B - \Sigma_B(\mathbf{p} = \mathbf{0}, i\omega_B = 0) = 0, \quad (6)$$

which states that the Bose excitations become gapless at the Bose-Einstein condensation (BEC) phase-transition temperature  $T_c$ .

We here present some notes on this *improved*  $T$ -matrix approximation (iTMA) [26].

(1) The ordinary TMA [25] uses the *bare* Bose Green's function  $G_B^0$  in Eq. (4), which has a gapped single-particle dispersion even at  $T_c$ . Because of this, TMA underestimates effects of low-energy Bose excitations near  $T_c$ . Thus, iTMA is considered to be valid for a wider temperature region than TMA.

(2) With increasing the interaction strength, the Fermi chemical potential  $\mu_F$  at low temperatures is expected to decrease from the Fermi energy  $\varepsilon_F$ , because most Fermi and Bose atoms eventually form bound molecules in the strong-coupling regime. While this behavior of  $\mu_F$  is really obtained in iTMA [26], TMA cannot describe this. In this sense, iTMA is applicable to a stronger coupling regime than TMA.

(3) However, iTMA still has room for improvement. For example, in evaluating the diagrams shown in Fig. 1, iTMA still employs the bare Fermi single-particle Green's function:

$$G_F^0(\mathbf{p}, i\omega_F) = \frac{1}{i\omega_F - \xi_p^F}. \quad (7)$$

We also recall that the modified Bose Green's function in Eq. (5) only involves the self-energy at  $\mathbf{q} = \nu_n = 0$ . Thus, in summing up the diagrams in Fig. 1, iTMA completely ignores many-body effects described by the dynamical part of the self-energy, such as quasiparticle damping, mass enhancement, as well as wave-function renormalization. [Note that the resulting dressed Green's function in Eq. (3) involves these effects.] In addition, judging from the knowledge about the BCS-BEC crossover phenomenon in a two-component Fermi gas [47], we find that an effective interaction between composite molecules is only partially taken into account through  $\Sigma_B(\mathbf{0}, 0)$  involved in  $\tilde{G}_B^0(\mathbf{p}, i\omega_B)$ . Such a molecular interaction described by  $\Sigma_F(\mathbf{p}, i\omega_F)$  and  $\Sigma_B(\mathbf{p} \neq \mathbf{0}, i\omega_B \neq 0)$  is ignored in iTMA. To overcome these deficiencies of iTMA, we need to employ the self-consistent  $T$ -matrix approximation [47], where all the Green's functions in Fig. 1 are replaced by the fully dressed ones. This extension remains as our future problem.

The summation of the diagrams in Fig. 1 gives

$$\Sigma_B(\mathbf{p}, i\omega_B) = T \sum_{\mathbf{q}, i\omega'_F} \Gamma_{BF}(\mathbf{q}, i\omega'_F) G_F^0(\mathbf{q} - \mathbf{p}, i\omega'_F - i\omega_B), \quad (8)$$

$$\Sigma_F(\mathbf{p}, i\omega_F) = -T \sum_{\mathbf{q}, i\omega'_F} \Gamma_{BF}(\mathbf{q}, i\omega'_F) \tilde{G}_B^0(\mathbf{q} - \mathbf{p}, i\omega'_F - i\omega_F), \quad (9)$$

where

$$\begin{aligned} \Gamma_{BF}(\mathbf{q}, i\omega_F) &= -\frac{U_{BF}}{1 - U_{BF}\Pi_{BF}(\mathbf{q}, i\omega_F)} \\ &= \frac{1}{\frac{m}{4\pi a_{BF}} + [\Pi_{BF}(\mathbf{q}, i\omega_F) - \sum_{\mathbf{p}} \frac{p_c}{p^2}]} \end{aligned} \quad (10)$$

is the iTMA Bose-Fermi scattering matrix, which physically describes heteropairing fluctuations. Here,

$$\begin{aligned} \Pi_{BF}(\mathbf{q}, i\omega_F) &= -T \sum_{\mathbf{p}, i\omega_B} G_F^0(\mathbf{q} - \mathbf{p}, i\omega_F - i\omega_B) \tilde{G}_B^0(\mathbf{p}, i\omega_B) \\ &= \sum_{\mathbf{p}} \frac{1 - f(\xi_{\mathbf{q}-\mathbf{p}}^F) + n(\xi_{\mathbf{p}}^B)}{\xi_{\mathbf{q}-\mathbf{p}}^F + \xi_{\mathbf{p}}^B - i\omega_F} \end{aligned} \quad (11)$$

is the heteropair correlation function, where  $n(x)$  and  $f(x)$  are the Bose and Fermi distribution function, respectively.

The BEC phase-transition temperature  $T_c$  is determined from the Hugenholtz-Pines condition in Eq. (6). We actually solve this equation, together with the equation for the number  $N_B$  ( $N_F$ ) of Bose (Fermi) atoms,

$$N_B = -T \sum_{\mathbf{p}, i\omega_B} G_B(\mathbf{p}, i\omega_B), \quad (12)$$

$$N_F = T \sum_{\mathbf{p}, i\omega_F} G_F(\mathbf{p}, i\omega_F), \quad (13)$$

to self-consistently determine  $T_c$ ,  $\mu_B(T_c)$ , and  $\mu_F(T_c)$ . Above  $T_c$ , we only deal with the number equations (12) and (13), to evaluate  $\mu_B(T)$  and  $\mu_F(T)$ .

The single-particle SW  $A_{s=B,F}(\mathbf{p}, \omega)$  is related to the analytic-continued Green's functions as

$$A_{s=B,F}(\mathbf{p}, \omega) = -\frac{1}{\pi} \text{Im}[G_s(\mathbf{p}, i\omega_s \rightarrow \omega + i\delta \equiv \omega_+)], \quad (14)$$

where  $\delta$  is an infinitesimally small positive number. The photoemission spectrum (PES)  $I_{s=B,F}(\mathbf{p}, \omega)$  [39–41] is then obtained from Eq. (14) [42,43], within the ignorance of the final-state interaction:

$$I_F(\mathbf{p}, \omega) = 2\pi t_s^2 p^2 A_F(\mathbf{p}, \omega) f(\omega), \quad (15)$$

$$I_B(\mathbf{p}, \omega) = 2\pi t_s^2 p^2 A_B(\mathbf{p}, \omega) n(\omega). \quad (16)$$

Here,  $t_s$  is a transfer-matrix element from the initial atomic hyperfine state  $|I\rangle$  to the final one  $|F\rangle$  ( $\neq |I\rangle$ ). Between the two, the Fermi SW will be found to be more useful for the study of many-body coupling phenomena mentioned in Sec. I. Thus, we only examine the Fermi PES in this paper.

### III. SINGLE-PARTICLE EXCITATIONS IN A POPULATION-IMBALANCED BOSE-FERMI MIXTURE

#### A. Outline and summary of main results in this section

In this section, we treat a Bose-Fermi mixture with population imbalance ( $N_B \neq N_F$ ). For simplicity, we set  $m_B = m_F$ . We first examine the BEC phase-transition temperature  $T_c$  in the presence of population imbalance. We then discuss single-particle excitations in a Bose-Fermi mixture with population imbalance. In this discussion we first consider the case at  $T_c$ , and then proceed to the case above  $T_c$ .

We summarize the main results obtained in this section.

(1) When  $N_B \leq N_F$ , we obtain a quantum critical point (QCP). When the interaction strength exceeds the QCP, the BEC phase transition no longer occurs.

(2) When the population difference is small ( $N_B \sim N_F$ ), we show that the Fermi SW  $A_F(\mathbf{p}, \omega)$  exhibits a triple-peak structure, describing Fermi atomic excitations, Bose atomic excitations, and Bose-Fermi molecular excitations. Such a structure is not clearly seen in the Bose SW  $A_B(\mathbf{p}, \omega)$ . The latter result is due to the fact that the detailed coupling mechanism of Bose atomic excitations with other excitation channels is somehow different from that of Fermi atomic excitations.

(3) When  $N_B/N_F \ll 1$ , both the atom-molecule and Fermi-Bose couplings become weak in the Fermi SW  $A_F(\mathbf{p}, \omega)$ , so that it exhibits a single-peak structure. In contrast, the atom-molecule coupling still remains when  $N_B/N_F \gg 1$ , leading to a double-peak structure in  $A_F(\mathbf{p}, \omega)$ . Our results in the highly population-imbalanced case are directly related to the Bose-polaron problem [36–38].

#### B. BEC phase-transition temperature $T_c$ and effects of population imbalance

Figure 2 shows the BEC transition temperature  $T_c$  in a Bose-Fermi mixture with population imbalance ( $N_B \neq N_F$ ). In this figure, the population imbalance is tuned by the

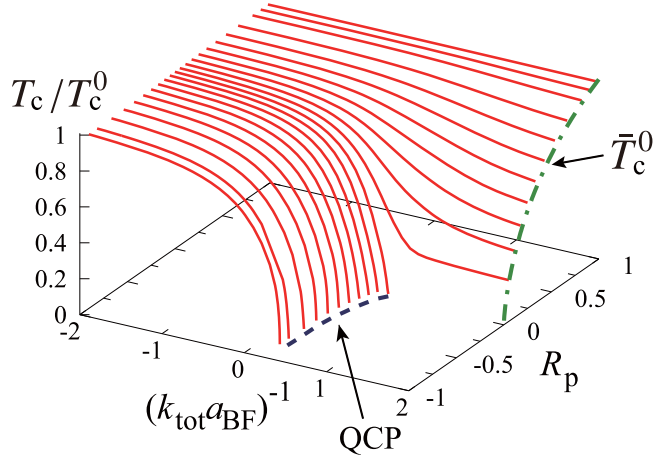


FIG. 2. Calculated Bose-Einstein condensation temperature  $T_c$  in a Bose-Fermi mixture with population imbalance ( $N_B \neq N_F$ ). The population imbalance is parametrized by  $R_p$  in Eq. (17):  $R_p > 0$  ( $R_p < 0$ ) corresponds to the case of  $N_B > N_F$  ( $N_B < N_F$ ). We set  $m_B = m_F$ . The dashed line shows  $\bar{T}_c^0$  in Eq. (19).  $T_c^0$  is the BEC phase-transition temperature in an ideal gas of  $N_B$  bosons in Eq. (18). “QCP” is the quantum critical point at which  $T_c$  vanishes.

polarization parameter:

$$R_p \equiv \frac{N_B - N_F}{N_B + N_F}. \quad (17)$$

In the weak-coupling limit  $(k_{\text{tot}} a_{\text{BF}})^{-1} \ll -1$ , since Fermi atoms do not affect the BEC phase transition,  $T_c$  is simply given by that in an ideal Bose gas:

$$T_c^0 = \frac{2\pi}{m_B} \left( \frac{N_B}{\zeta(3/2)} \right)^{2/3}, \quad (18)$$

where  $\zeta(3/2) \simeq 2.613$  is the zeta function. Starting from this case, when  $N_B < N_F$  ( $R_p < 0$ ), we see in Fig. 2 that the overall interaction dependence of  $T_c$  is similar to that in the population-balanced case ( $N_B = N_F$ ) [26]:  $T_c$  gradually decreases from  $T_c^0$  with increasing the interaction strength, to eventually vanish around the unitary limit  $(k_{\text{tot}} a_{\text{BF}})^{-1} = 0$ . This vanishing  $T_c$  is due to the formation of Bose-Fermi molecules at the two-body level, and the most Bose atoms pair up with Fermi atoms to become composite molecules there. As a result, BEC of unpaired *Bose atoms* no longer occurs, when the interaction strength exceeds the QCP [ $(k_{\text{tot}} a_{\text{BF}})^{-1} \sim 0$ ], as seen in Fig. 2.

When  $N_B > N_F$  ( $R_p > 0$ ), the BEC phase transition remains to exist ( $T_c > 0$ ) even in the strong-coupling limit [ $(k_{\text{tot}} a_{\text{BF}})^{-1} \gg +1$ ]. This is simply because as many as  $\Delta N_B \equiv N_B - N_F (> 0)$  bosons remain unpaired in this limit. Indeed, as shown in Fig. 2,  $T_c$  in the strong-coupling limit is well described by their BEC transition temperature  $\bar{T}_c^0$ :

$$\bar{T}_c^0 = \frac{2\pi}{m_B} \left( \frac{\Delta N_B}{\zeta(3/2)} \right)^{2/3}. \quad (19)$$

### C. Single-particle spectral weight $A_{s=F,B}(p, \omega)$ at $T_c$

Figures 3(a1)–3(a5) show the Fermi SW  $A_F(p, \omega)$  in the unitary limit at  $T_c$ . In the population-balanced case

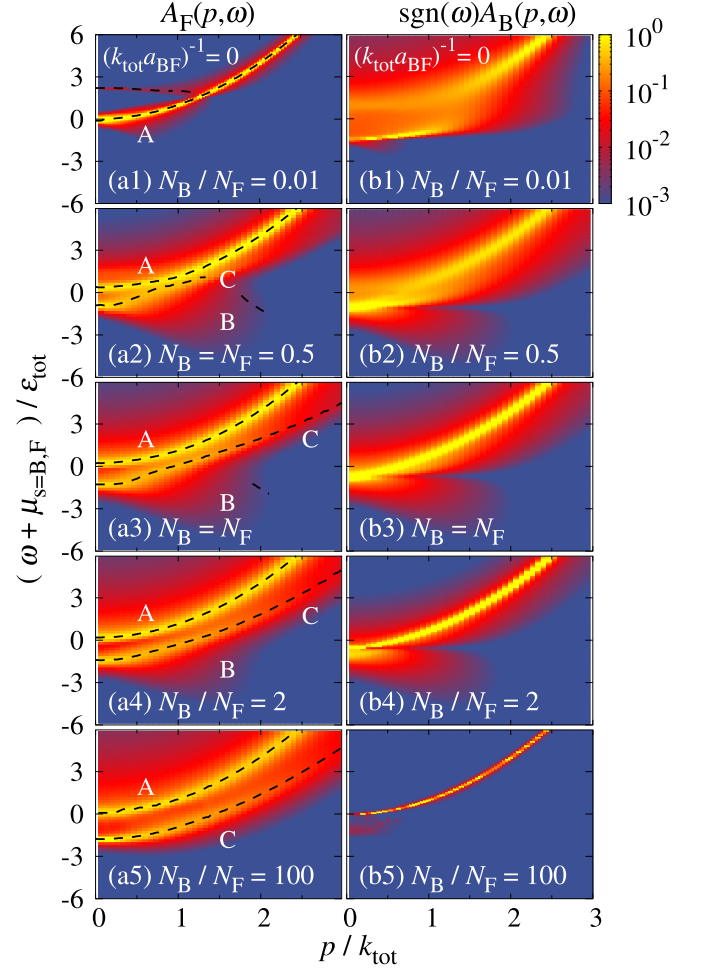


FIG. 3. Calculated intensity of single-particle spectral weights  $A_{s=B,F}(p, \omega)$  in a population-imbalanced unitary Bose-Fermi mixture at  $T = T_c$ . (a1–a5)  $A_F(p, \omega)$ . (b1–b5)  $A_B(p, \omega) \times \text{sgn}(\omega)$ . We set  $m_B = m_F$ . The spectral intensity is normalized by  $\epsilon_{\text{tot}}^{-1} \equiv 2m/k_{\text{tot}}^2$ . In the left panels, we plot the dashed lines along the spectral peak positions for an eye guide.

[Fig. 3(a3)], the Fermi SW exhibits a triple-peak structure as a result of the Fermi-Bose and atom-molecule couplings [26] mentioned in Sec. I: (A) a sharp peak line along the Fermi free particle dispersion,  $\omega = \xi_p^F$ ; (B) a broad downward peak in the negative-energy region around  $\omega = -\tilde{\xi}_p^B$ , where the Bose dispersion  $\tilde{\xi}_p^B$  is given below Eq. (5); and (C) a sharp upward peak line along the composite molecular dispersion,  $\omega = \xi_p^{\text{CF}} \equiv p^2/(2M_{\text{CF}}) - \mu_{\text{CF}}$ , where  $M_{\text{CF}} \simeq m_B + m_F$  is a molecular mass and  $\mu_{\text{CF}}$  is the molecular chemical potential [48].

When the ratio  $N_B/N_F$  decreases from unity [decreasing from Fig. 3(a3) to Fig. 3(a1)], peaks B and C gradually disappear. This is simply because the system approaches a free Fermi gas. In the highly population-imbalanced case in Fig. 3(a1), the peak line (A) is only seen, as expected. In the opposite case, with increasing the ratio  $N_B/N_F > 1$ , while the broad peak (B) gradually disappears, the molecular peak (C) continues to exist, in addition to the free fermion dispersion (A), even in Fig. 3(a5).

#### D. Explanation for atom-molecule and Bose-Fermi coupling phenomena

To understand these population-imbalance effects on the Fermi SW, we approximately treat the Bose-Fermi scattering matrix  $\Gamma_{\text{BF}}(\mathbf{q}, i\omega_{\text{F}})$  in Eq. (10) as the composite molecular propagator [26]:

$$\Gamma_{\text{BF}}(\mathbf{q}, i\omega_{\text{F}}) \simeq \frac{Z}{i\omega_{\text{F}} - \xi_{\mathbf{q}}^{\text{CF}}}, \quad (20)$$

where  $Z (>0)$  is the renormalization factor. Strictly speaking, this approximation is justified only in the strong-coupling limit [where one finds  $Z = 8\pi^2/(m^2 a_{\text{BF}})$  [26]]; however, even not in this extreme limit, Eq. (20) is still useful in considering how heteropairing fluctuations affect single-particle excitations. Substituting Eq. (20) into the self-energy  $\Sigma_{\text{F}}(\mathbf{p}, i\omega_{\text{F}})$  in Eq. (9), and carrying out the  $\omega'_{\text{F}}$  summation, we obtain

$$\begin{aligned} \Sigma_{\text{F}}(\mathbf{p}, i\omega_{\text{F}}) &= Z \sum_{\mathbf{q}} \left[ \frac{n(\tilde{\xi}_{\mathbf{q}}^{\text{B}})}{i\omega_{\text{F}} - \xi_{\mathbf{p}-\mathbf{q}}^{\text{CF}} + \tilde{\xi}_{\mathbf{q}}^{\text{B}}} + \frac{f(\xi_{\mathbf{q}}^{\text{CF}})}{i\omega_{\text{F}} + \tilde{\xi}_{\mathbf{p}-\mathbf{q}}^{\text{B}} - \xi_{\mathbf{q}}^{\text{CF}}} \right] \\ &\simeq \frac{ZN_{\text{B}}^0}{i\omega_{\text{F}} - \xi_{\mathbf{p}}^{\text{CF}}} + \left\langle \frac{ZN_{\text{CF}}}{i\omega_{\text{F}} + \tilde{\xi}_{\mathbf{k}_{\text{CF}}-\mathbf{p}}^{\text{B}}} \right\rangle_{\mathbf{k}_{\text{CF}}}. \end{aligned} \quad (21)$$

Here,  $N_{\text{CF}} = \sum_{\mathbf{q}} f(\xi_{\mathbf{q}}^{\text{CF}})$  is the number of composite Fermi molecules with the chemical potential  $\mu_{\text{CF}} > 0$ ,  $N_{\text{B}}^0 = \sum_{\mathbf{q}} n(\tilde{\xi}_{\mathbf{q}}^{\text{B}})$ , and  $|\mathbf{k}_{\text{CF}}| = \sqrt{2M_{\text{CF}}\mu_{\text{CF}}}$  gives the size of the Fermi surface in the composite Fermi molecular gas. The average  $\langle \dots \rangle_{\mathbf{Q}}$  is taken over the direction of  $\mathbf{Q}$ . In the last expression of Eq. (21), we have approximately set  $\mathbf{q} = 0$  in the denominator of the first term, by using the fact that the Bose distribution function  $n(\tilde{\xi}_{\mathbf{q}}^{\text{B}})$  diverges at  $\mathbf{q} = 0$  at  $T_c$ . In the last term, we have also approximated  $\mathbf{q}$  in the denominator to  $\mathbf{k}_{\text{CF}}$ , by noting that the region near the Fermi surface of the composite Fermi molecules is important.

We comment on the difference between the two terms in the last line of Eq. (21). Between the two, the factor  $N_{\text{B}}^0$  in the first term physically means that unpaired free Bose atoms contribute to the coupling between a Fermi atom and a composite Fermi molecule. In this case, because the Bose atoms around  $\mathbf{q} = 0$  dominantly contribute to this coupling phenomenon, a Fermi atom with momentum  $\mathbf{p}$  couples with a composite Fermi molecule with the same momentum  $\mathbf{p}$ , as seen in the first term of Eq. (21). Because of this, the angular integration is absent in this term. On the other hand, the factor  $N_{\text{CF}}$  in the last term indicates that the coupling between Fermi and Bose atoms is dominated by the composite Fermi molecules. In this case, the region near the Fermi surface of these molecules is expected to be crucial for this coupling phenomenon. That is, Fermi molecules with various directions of the Fermi momentum  $\mathbf{k}_{\text{CF}}$  contribute to this coupling phenomenon. As a result, a Fermi atom with momentum  $\mathbf{p}$  couples with Bose atoms with various kinetic energies  $\tilde{\xi}_{\mathbf{k}_{\text{CF}}-\mathbf{p}}^{\text{B}}$ , leading to the angular integration of  $\mathbf{k}_{\text{CF}}$  in Eq. (21). Because of this, Bose excitations give a broad spectral structure in the negative-energy region of the Fermi SW [see, for example, Fig. 3(a3)].

Substituting Eq. (21) into Eq. (3), we obtain [26]

$$\begin{aligned} G_{\text{F}}(\mathbf{p}, i\omega_{\text{F}} \rightarrow \omega_{+}) \\ \simeq \frac{1}{\omega_{+} - \xi_{\mathbf{p}}^{\text{F}} - \frac{ZN_{\text{B}}^0}{\omega_{+} - \tilde{\xi}_{\mathbf{p}}^{\text{B}}} - \left\langle \frac{ZN_{\text{CF}}}{\omega_{+} + \tilde{\xi}_{\mathbf{k}_{\text{CF}}-\mathbf{p}}^{\text{B}}} \right\rangle_{\mathbf{k}_{\text{CF}}}}. \end{aligned} \quad (22)$$

Equation (22) explains that heteropairing fluctuations couple the Fermi atomic excitations  $\omega = \xi_{\mathbf{p}}^{\text{F}}$  (A) with the molecular excitations  $\omega = \xi_{\mathbf{p}}^{\text{CF}}$  (C) with the coupling strength  $ZN_{\text{B}}^0$ , as well as with the Bose excitations  $\omega = -\tilde{\xi}_{\mathbf{k}_{\text{CF}}-\mathbf{p}}^{\text{B}}$  (B) with the coupling strength  $ZN_{\text{CF}}$ .

When the number of Bose atoms decreases ( $N_{\text{B}}/N_{\text{F}} < 1$ ), both  $N_{\text{B}}^0$  and  $N_{\text{CF}}$  in the denominator in Eq. (22) decrease, to eventually vanish in the limit  $N_{\text{B}} \rightarrow 0$ . This immediately explains the single-peak structure in the Fermi SW in Fig. 3(a1). When  $N_{\text{F}}$  decreases ( $N_{\text{B}}/N_{\text{F}} > 1$ ), while  $N_{\text{CF}}$  vanishes in the large population-imbalance limit,  $N_{\text{B}}^0$  approaches the nonzero value  $N_{\text{B}}$ . Thus, Eq. (22) is reduced to

$$G_{\text{F}}(\mathbf{p}, \omega_{+}) = \frac{1}{\omega_{+} - \xi_{\mathbf{p}}^{\text{F}} - \frac{ZN_{\text{B}}}{\omega_{+} - \xi_{\mathbf{p}}^{\text{CF}}}}, \quad (23)$$

which has the two poles

$$E_{\mathbf{p}}^{\pm} = \frac{1}{2} \left[ \xi_{\mathbf{p}}^{\text{F}} + \xi_{\mathbf{p}}^{\text{CF}} \right] \pm \sqrt{\left[ \xi_{\mathbf{p}}^{\text{F}} - \xi_{\mathbf{p}}^{\text{CF}} \right]^2 + 4ZN_{\text{B}}}. \quad (24)$$

Equation (24) explains the double-peak structure in Fig. 3(a5). That is, the Fermi single-particle excitations in the highly population-imbalanced regime ( $N_{\text{B}}/N_{\text{F}} \gg 1$ ) are dominated by the atom-molecule coupling phenomenon.

Applying the same approximation to the Bose component, we obtain [26,49]

$$\begin{aligned} G_{\text{B}}(\mathbf{p}, i\omega_{\text{F}} \rightarrow \omega_{+}) \\ \simeq \frac{1}{\omega_{+} - \xi_{\mathbf{p}}^{\text{B}} - \left\langle \frac{ZN_{\text{F}}^0}{\omega_{+} - \tilde{\xi}_{\mathbf{k}_{\text{F}}-\mathbf{p}}^{\text{F}}} \right\rangle_{\mathbf{k}_{\text{F}}} - \left\langle \frac{ZN_{\text{CF}}}{\omega_{+} + \tilde{\xi}_{\mathbf{k}_{\text{CF}}-\mathbf{p}}^{\text{B}}} \right\rangle_{\mathbf{k}_{\text{CF}}}}. \end{aligned} \quad (25)$$

Here,  $N_{\text{F}}^0 = \sum_{\mathbf{q}} f(\xi_{\mathbf{q}}^{\text{F}})$ , and  $|\tilde{\mathbf{k}}_{\text{F}}| = \sqrt{2m_{\text{F}}\mu_{\text{F}}}$ . Equation (25) shows that the Bose single-particle excitations ( $\omega = \xi_{\mathbf{p}}^{\text{B}}$ ) couple with composite Fermi molecular excitations ( $\omega = \xi_{\mathbf{k}_{\text{F}}-\mathbf{p}}^{\text{CF}}$ ), as well as Fermi hole excitations ( $\omega = -\tilde{\xi}_{\mathbf{k}_{\text{CF}}-\mathbf{p}}^{\text{B}}$ ); however, because of the angular averages in the denominator of Eq. (25), the triple-peak structure is not clearly seen in the Bose SW  $A_{\text{B}}(\mathbf{p}, \omega)$ , when  $N_{\text{B}} = N_{\text{F}}$  [see Fig. 3(b3)].

When the number  $N_{\text{F}}$  of Fermi atoms decreases ( $N_{\text{B}}/N_{\text{F}} > 1$ ), both  $N_{\text{F}}^0$  and  $N_{\text{CF}}$  decrease. Thus, the Bose SW is gradually reduced to that in a free Bose gas (where the single peak line is along  $\omega = \xi_{\mathbf{p}}^{\text{B}}$ ), as seen in Figs. 3(b3)–3(b5). With increasing  $N_{\text{F}}$  ( $N_{\text{B}}/N_{\text{F}} < 1$ ), the system eventually reaches the situation that  $N_{\text{F}}^0 \rightarrow N_{\text{F}} \gg N_{\text{CF}} \sim N_{\text{B}}^0$ . Because of this, the spectral structures in Figs. 3(b1) and 3(b2) are dominated by Bose atomic excitations and broad composite molecular excitations, but the downward broad peak associated with Fermi hole excitations becomes weak.

The above discussions indicate that the Fermi SW  $A_{\text{F}}(\mathbf{p}, \omega)$  is more suitable than the Bose SW  $A_{\text{B}}(\mathbf{p}, \omega)$ , for the study of the Fermi-Bose and atom-molecule coupling phenomena.

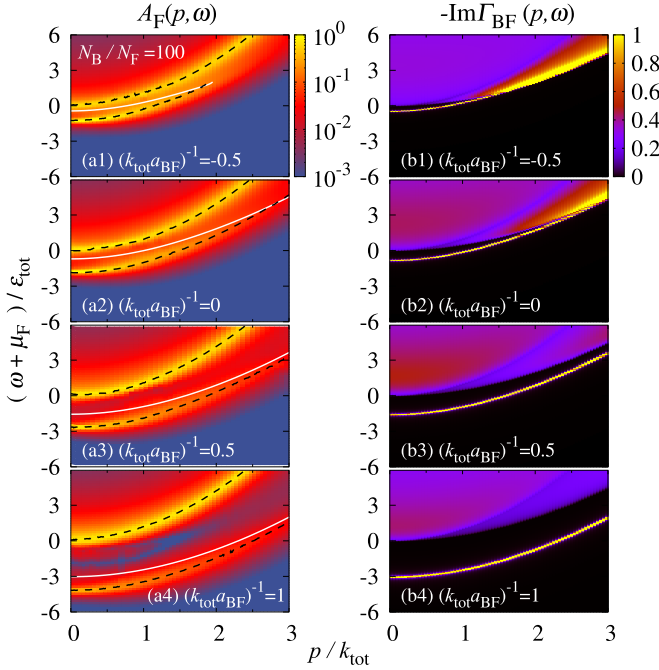


FIG. 4. (a1–a4) Calculated intensity of the Fermi SW  $A_F(\mathbf{p}, \omega)$  in a highly population-imbalanced Bose-Fermi mixture ( $N_B/N_F = 100 \gg 1$ ) at  $T_c$ . We take  $m_B = m_F$ . The spectral intensity is normalized by  $\varepsilon_{\text{tot}}^{-1}$ . In each left panel, the black dashed lines show the peak positions of  $A_F(\mathbf{p}, \omega)$ . The white solid line shows the peak position of the spectrum of the Bose-Fermi scattering matrix  $-\text{Im}[\Gamma_{\text{BF}}(\mathbf{q}, i\omega_F \rightarrow \omega_+)]$  shown in (b1)–(b4). In the left panels, the intensity is normalized by  $2\pi^2/(mk_{\text{tot}})$ .

### E. Relation to the Bose-polaron problem in the highly population-imbalanced case

We point out that the highly population-imbalanced case ( $N_B/N_F \gg 1$ ) is related to the Bose-polaron system [36–38,50]. To clearly see this, we note that, in the strong-coupling limit, the quasiparticle dispersions  $E_p^\pm$  in Eq. (24) are reduced to

$$\begin{cases} E_p^+ = \xi_p^F + \frac{4\pi a_{\text{BF}}}{m} N_B, \\ E_p^- = \xi_p^{\text{CF}} - \frac{4\pi a_{\text{BF}}}{m} N_B. \end{cases} \quad (26)$$

These are the same as the polaron energies obtained in Ref. [50]:  $E_p^+$  represents an atomlike quasiparticle, which repulsively interacts with surrounding bosons (repulsive polaron). In addition, in the presence of a bound state, there exists another scattering process where a composite Fermi molecule ( $\omega = \xi_p^{\text{CF}}$ ) appears in the intermediate state. This process causes an additional quasiparticle with the dispersion  $E_p^-$ , which attractively interacts with surrounding bosons. In Ref. [50], it is referred to as the attractive polaron.

Figures 4(a1)–4(a4) show that the atom-molecule coupling phenomenon seen in Fig. 3(a5) also occurs away from the unitary limit: Because a two-body bound state is formed in the strong-coupling regime [ $(k_{\text{tot}} a_{\text{BF}})^{-1} > 0$ ], the appearance of the lower sharp peak in Figs. 4(a3) and 4(a4) would be reasonable. However, we also see a sharp molecular peak line in Fig. 4(a1), in spite of the absence of a two-body bound state when  $(k_{\text{tot}} a_{\text{BF}})^{-1} = -0.5 < 0$ .

Regarding this, when we plot the spectrum  $\text{Im}[\Gamma_{\text{BF}}(\mathbf{p}, i\omega_F \rightarrow \omega_+)]$  of the Bose-Fermi scattering matrix, one finds an isolated sharp peak line below the continuum spectrum, not only in the strong-coupling side where  $(k_{\text{tot}} a_{\text{BF}})^{-1} \geq 0$  [Figs. 4(b2)–4(b4)], but also in the weak-coupling side where  $(k_{\text{tot}} a_{\text{BF}})^{-1} < 0$  [Fig. 4(b1)]. Because the formation of a two-body bound state does not occur when  $(k_{\text{tot}} a_{\text{BF}})^{-1} < 0$ , Fig. 4(b1) implies the stabilization of a Bose-Fermi bound state by a many-body (medium) effect.

To see this many-body effect in a simple manner, we approximate Eq. (10) at  $T_c$  to

$$\Gamma_{\text{BF}}(\mathbf{q}, \omega_+) \simeq \frac{1}{\frac{m}{4\pi a_{\text{BF}}} + \sum_{\mathbf{p}} \left[ \frac{1}{\varepsilon_{\mathbf{q}-\mathbf{p}}^F + \varepsilon_{\mathbf{p}}^B - \tilde{\omega}_+} - \frac{m}{p^2} \right] - N_B^0 G_F^0(\mathbf{q}, \omega_+)}, \quad (27)$$

where  $\tilde{\omega} = \omega + \mu_F$ , and we have taken the analytic continuation  $i\omega_F \rightarrow \omega_+$ . When we ignore the last term in the denominator of Eq. (27), the condition for the pole of this equation,

$$\frac{m}{4\pi a_{\text{BF}}} + \sum_{\mathbf{p}} \left[ \frac{1}{\varepsilon_{\mathbf{q}-\mathbf{p}}^F + \varepsilon_{\mathbf{p}}^B - \tilde{\omega}_+} - \frac{m}{p^2} \right] = 0, \quad (28)$$

is essentially the same as the two-body bound-state equation, which only has a solution when  $a_{\text{BF}} > 0$ . Thus, the term  $N_B^0 G_F^0(\mathbf{q}, \omega_+)$  in Eq. (27) may be interpreted as a many-body (medium) correction to the bound state. Including this correction term, we obtain the pole equation of Eq. (27) at  $\mathbf{q} = 0$  as, after carrying out the  $\mathbf{p}$  summation,

$$\frac{m}{4\pi a_{\text{BF}}} - \frac{m^{\frac{3}{2}}}{4\pi} \sqrt{|\tilde{\omega}|} + \frac{N_B^0}{|\tilde{\omega}|} = 0. \quad (29)$$

The pole equation (29) has a bound-state solution even when  $(k_{\text{tot}} a_{\text{BF}})^{-1} \leq 0$  [24]. For example, at unitarity ( $a_{\text{BF}}^{-1} = 0$ ), Eq. (29) gives

$$\tilde{\omega} = -\frac{(4\pi N_B^0)^{\frac{2}{3}}}{m}. \quad (30)$$

The above discussion explains the reason why the sharp peak line appears below the continuum of the spectrum  $\text{Im}[\Gamma_{\text{BF}}(\mathbf{p}, i\omega_F \rightarrow \omega_+)]$  in all the right panels in Fig. 4. We also see in Figs. 4(a1)–4(a4) that the lower spectral peak of  $A_F(\mathbf{p}, \omega)$  (black dashed line) is close to this sharp peak line (white solid line). The reason why the former is somehow pushed down from the latter is due to the coupling with the Fermi atomic excitations  $\omega = \xi_p^F$  [see  $E_p^-$  in Eq. (24)].

The above discussions are also applicable to the population-balanced case ( $N_B = N_F$ ): In Fig. 5, the spectrum  $-\text{Im}[\Gamma_{\text{BF}}(\mathbf{p}, i\omega_F \rightarrow \omega_+)]$  of the Bose-Fermi scattering matrix (right panels) has an isolated sharp peak. In these panels, the peak energy is lowered as the interaction strength increases, because of the increase of the binding energy of a Bose-Fermi bound state. This tendency is the same as the highly population-imbalanced case shown in Fig. 4. This bound-state peak in  $\Gamma_{\text{BF}}(\mathbf{p}, i\omega_F \rightarrow \omega_+)$  brings about the lower peak in the Fermi SW  $A_F(\mathbf{p}, \omega)$ , as shown in the left panels.

To conclude, the character of a Bose-Fermi molecule continuously changes from a many-body bound state assisted

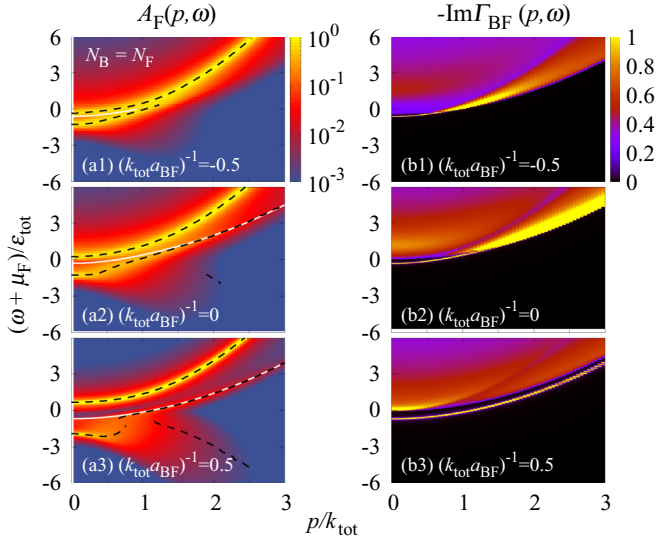


FIG. 5. Same plot as Fig. 4 for the population-balanced case  $N_B = N_F$ .

by a medium to a two-body bound state with increasing the strength of a heteropairing interaction. We briefly note that a similar crossover phenomenon from a polaron state to the two-body bound state (polaron-molecule crossover) has been discussed in the Bose-polaron system at  $T = 0$  [50].

### E. Single-particle spectral weight $A_{s=F,B}(p, \omega)$ above $T_c$

In the normal state above  $T_c$ , we expect the following two thermal effects.

(1) The Bose distribution function  $n(\xi_q^B)$  no longer diverges at  $q = 0$ , so that the approximation giving the first term in

the last line of Eq. (21) becomes worse. Roughly speaking, this would lead to the broadening of the peak line coming from molecular excitations in the Fermi SW  $A_F(p, \omega)$ . In addition, because the factor  $ZN_B^0 = Z \sum_q n_B(\xi_q^B)$  decreases with increasing temperature, the atom-molecule coupling also becomes weak.

(2) When Bose-Fermi bound states thermally dissociate into unpaired atoms at high temperatures, the approximate expression for the Bose-Fermi scattering matrix  $\Gamma_{BF}(q, i\omega_F)$  in Eq. (20) is no longer valid.

Keeping these two thermal effects in mind, we find in Figs. 6(a1)–6(a3) [ $(k_{\text{tot}}a_{BF})^{-1} = -0.5 < 0$ ] that the molecular peak line soon becomes obscure with increasing temperature above  $T_c$ . In this case, because of the weak Bose-Fermi pairing interaction, the sharp spectral peak in  $-\text{Im}[\Gamma_{BF}(q, i\omega_F \rightarrow \omega_+)]$  describing molecular excitations also soon disappears above  $T_c$  [see Figs. 6(b1)–6(b3)]. Thus, the above-mentioned two thermal effects are considered to suppress the atom-molecule coupling in the Fermi SW  $A_F(p, \omega)$  in the weak-coupling case.

In the strong-coupling regime [ $(k_{\text{tot}}a_{BF})^{-1} = 0.5 > 0$ ], Figs. 6(d1)–6(d3) indicate that the molecular spectrum still remains even at  $T/T_c^0 = 2.5$ , because of large molecular binding energy. In this case, thermal effects on the atom-molecule coupling are dominated by thermal effect 1 in the above discussion. Indeed, in Figs. 6(c1)–6(c3), while the molecular peak line gradually becomes broad with increasing temperature, the existence of this coupling phenomenon itself can still be confirmed in  $A_F(p, \omega)$  even at  $T/T_c^0 = 2.5$  Fig. 6(c3)].

Figure 6 indicates that, when we use the Fermi SW to examine the crossover from the medium-assisted (many-body) bound state in the weak-coupling regime to the two-body bound state in the strong-coupling regime in a

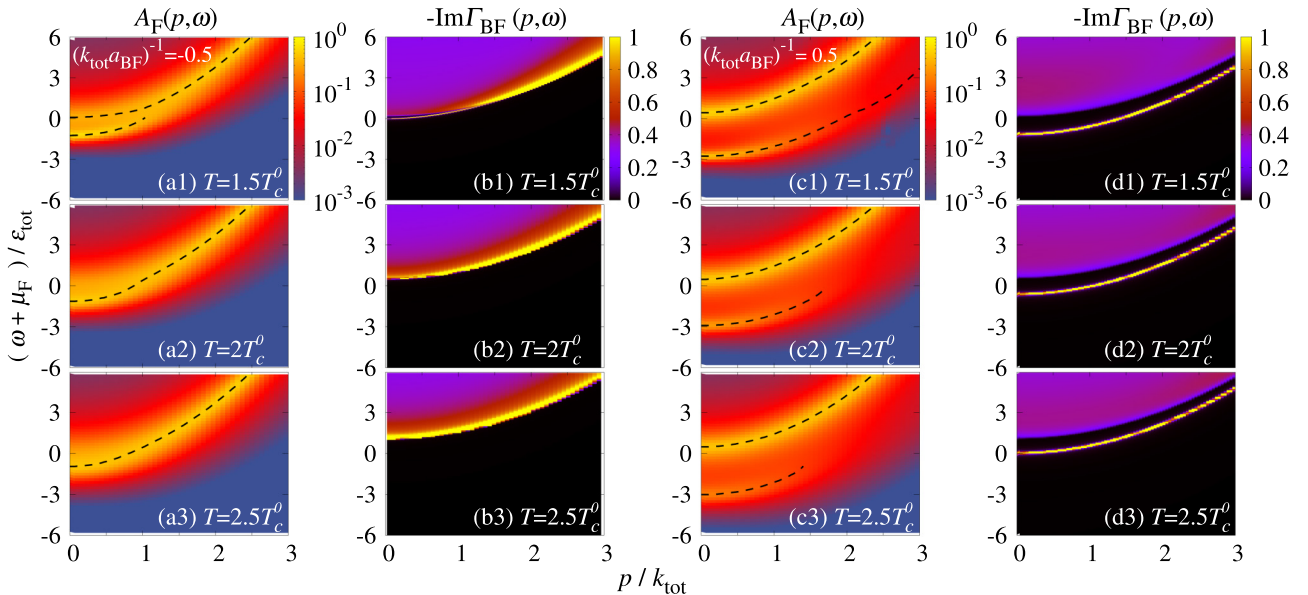


FIG. 6. Intensity of the Fermi SW  $A_F(p, \omega)$ , as well as the spectrum  $-\text{Im}[\Gamma_{BF}(q, i\omega_F \rightarrow \omega_+)]$  of the Bose-Fermi scattering matrix, in a highly population-imbalanced Bose-Fermi mixture ( $N_B/N_F = 100$ ). The dashed lines show the peak positions of  $A_F(p, \omega)$ . The normalization of the spectral intensity is the same as that in Fig. 4. (a1–a3, b1–b3) Weak-coupling case  $(k_{\text{tot}}a_{BF})^{-1} = -0.5$ . (c1–c3, d1–d3) Strong-coupling case  $(k_{\text{tot}}a_{BF})^{-1} = 0.5$ .

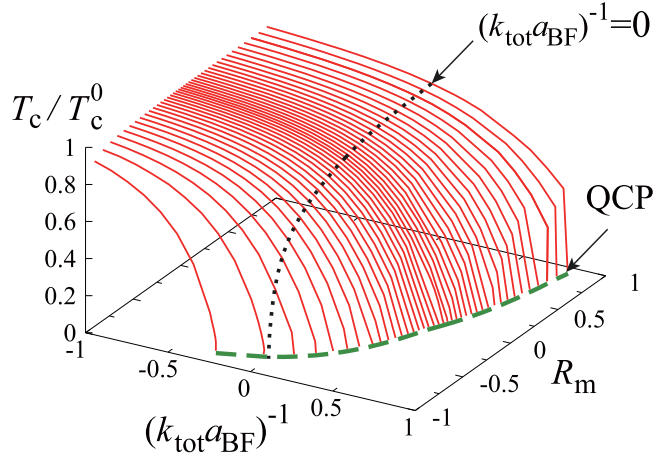


FIG. 7. Calculated BEC phase-transition temperature  $T_c$  in a Bose-Fermi mixture with mass imbalance. We set  $N_B = N_F$ . The parameter  $R_m$  is defined in Eq. (31):  $R_m > 0$  ( $R_m < 0$ ) corresponds to the case of  $m_F > m_B$  ( $m_F < m_B$ ). The dashed line is the quantum critical point (QCP) at which  $T_c$  vanishes.  $T_c^0$  is the BEC phase-transition temperature in an ideal Bose gas given in Eq. (18).

highly population-imbalanced Bose-Fermi mixture, we need to set the temperature near  $T_c$  in order to observe the former bound state.

#### IV. SINGLE-PARTICLE PROPERTIES OF THE MASS-IMBALANCED BOSE-FERMI MIXTURE

##### A. Outline and summary of main results in this section

In this section, we consider a Bose-Fermi mixture with mass imbalance ( $m_B \neq m_F$ ). We take  $N_B = N_F$ . We first determine  $T_c$  as a function of the interaction strength and the mass-imbalance parameter  $R_m$  defined in Eq. (31) below. We then discuss strong-coupling corrections to the Fermi and Bose SWs in a unitary Bose-Fermi mixture at  $T_c$ , in the presence of mass imbalance.

The main results obtained in this section are as follows.

(1) The QCP is always obtained in the mass-imbalanced case when  $N_B = N_F$ . We also find that the competition between the BEC phase transition of Bose atoms and the formation of Bose-Fermi composite molecules physically determines the critical interaction strength  $(k_{\text{tot}} a_{\text{BF}}^c)^{-1}$  at which  $T_c$  vanishes.

(2) As in the population-imbalanced case, the Fermi SW  $A_F(\mathbf{p}, \omega)$  is more useful than the Bose SW  $A_B(\mathbf{p}, \omega)$  for the study of mass-imbalance effects on atom-molecule and Bose-Fermi coupling phenomena. Among the three peak lines seen in the Fermi SW  $A_F(\mathbf{p}, \omega)$  at  $m_F = m_B$ , the Fermi atomic and Bose atomic branches remain when  $m_B/m_F \gg 1$ . In the opposite case ( $m_B/m_F \ll 1$ ), the Fermi atomic and Bose-Fermi molecular dispersions remain in  $A_F(\mathbf{p}, \omega)$ . These two results continuously change from one to the other, as the ratio  $m_B/m_F$  varies.

##### B. $T_c$ in the presence of mass imbalance

Figure 7 shows the BEC phase-transition temperature  $T_c$  and effects of mass imbalance in a Bose-Fermi mixture, where

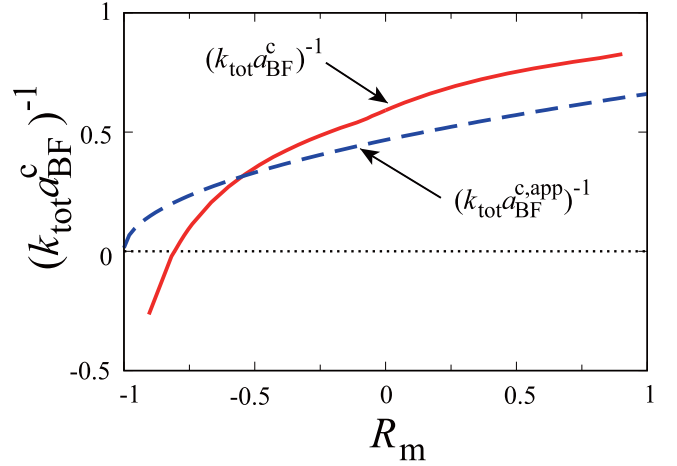


FIG. 8. Critical interaction strength  $(k_{\text{tot}} a_{\text{BF}}^c)^{-1}$ , which is defined as the interaction strength at which  $T_c$  vanishes, in a mass-imbalanced Bose-Fermi mixture. The dashed line shows the approximate result  $(k_{\text{tot}} a_{\text{BF}}^{c,\text{app}})^{-1}$  in Eq. (33). We set  $N_B = N_F$ .

mass difference is parametrized by

$$R_m = \frac{m_F - m_B}{m_F + m_B}. \quad (31)$$

In this figure,  $T_c$  gradually decreases from the ideal Bose-gas value  $T_c^0$  in Eq. (18) with increasing the Bose-Fermi interaction strength, to eventually vanish at a certain interaction strength (the QCP). Although this phenomenon has already been known in the mass-balanced case [25,26], Fig. 7 indicates that this suppression effect is more (less) remarkable, when  $m_B/m_F > 1$  ( $m_B/m_F < 1$ ). To clearly show this, we plot in Fig. 8 the critical interaction strength ( $\equiv (k_{\text{tot}} a_{\text{BF}}^c)^{-1}$ ) at which  $T_c$  vanishes.

To understand this mass-imbalance effect on  $T_c$ , we note that the BEC phase transition must occur before Bose atoms form Bose-Fermi bound states by the heteropairing interaction  $-U_{\text{BF}}$ : In the strong-coupling side  $(k_{\text{tot}} a_{\text{BF}})^{-1} > 0$ , the characteristic temperature below which the bound molecules appear is given by the binding energy  $E_{\text{bind}}^{2b}$  of a two-body bound state, given by

$$E_{\text{bind}}^{2b} = \frac{1}{m a_{\text{BF}}^2}, \quad (32)$$

where  $m$  is given below Eq. (2). Thus, the BEC phase transition would not occur, when the bare BEC transition temperature  $T_c^0 (\propto m_B^{-1})$  in Eq. (18) is much lower than  $E_{\text{bind}}^{2b}$ . Using this discussion, we can approximately estimate the critical interaction strength ( $\equiv a_{\text{BF}}^{c,\text{app}}$ ) at the QCP from the condition  $T_c^0 \simeq E_{\text{bind}}^{2b}$ , which gives

$$\begin{aligned} (k_{\text{tot}} a_{\text{BF}}^{c,\text{app}})^{-1} &= \left( \frac{4}{3\sqrt{\pi}\zeta(3/2)} \right)^{1/3} \frac{1}{\sqrt{1 + m_B/m_F}} \\ &= 0.66 \frac{1}{\sqrt{1 + m_B/m_F}}. \end{aligned} \quad (33)$$

Because Eq. (33) assumes a two-body bound state, it is only valid for  $(k_{\text{tot}} a_{\text{BF}}^{c,\text{app}})^{-1} > 0$ . However, a many-body bound state actually exists in the weak-coupling side

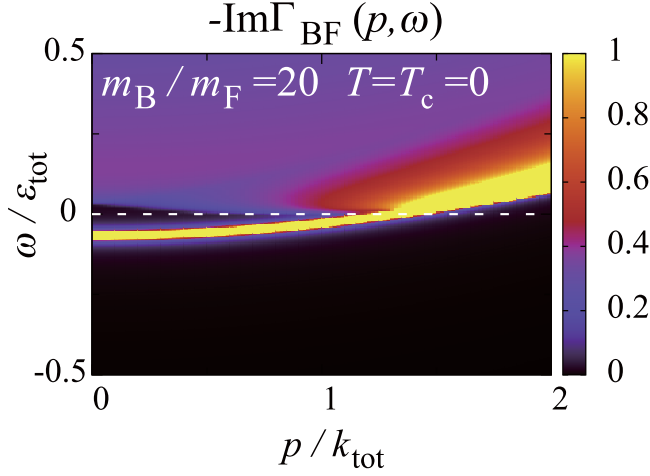


FIG. 9. Spectral intensity  $-\text{Im}[\Gamma_{\text{BF}}(q, i\omega_F \rightarrow \omega_+)]$  of the Bose-Fermi scattering matrix in a highly mass-imbalanced Bose-Fermi mixture ( $m_B/m_F = 20$ , or  $R_m \simeq -0.9$ ). We take the interaction strength  $(k_{\text{tot}}a_{\text{BF}})^{-1}$  to be equal to the critical value  $(k_{\text{tot}}a_{\text{BF}}^c)^{-1} = -0.25$  at which  $T_c$  vanishes.

$(k_{\text{tot}}a_{\text{BF}})^{-1} \leq 0$  [24,51]. For example, Fig. 9 shows the spectrum  $-\text{Im}[\Gamma_{\text{BF}}(\mathbf{p}, i\omega_F \rightarrow \omega_+)]$  of a Bose-Fermi scattering matrix in the highly mass-imbalanced case ( $m_B/m_F = 20 \gg 1$ ) at the critical interaction strength  $(k_{\text{tot}}a_{\text{BF}}^c)^{-1} = -0.25 < 0$  ( $T = 0$ ). In this figure, an isolated molecular branch is seen below the continuum, as in the population-imbalanced case (see Figs. 4–6). This many-body bound state in the weak-coupling region [ $(k_{\text{tot}}a_{\text{BF}})^{-1} \leq 0$ ] naturally explains why the critical coupling  $(k_{\text{tot}}a_{\text{BF}}^c)^{-1}$  can be negative in Fig. 8.

Apart from the weak-coupling side  $(k_{\text{tot}}a_{\text{BF}}^c)^{-1} < 0$ , the overall behavior of  $(k_{\text{tot}}a_{\text{BF}}^c)^{-1}$  shown in Fig. 8 is consistent with Eq. (33). This indicates that the competition between the BEC transition of Bose atoms and the formation of composite Bose-Fermi molecules determines the QCP.

### C. Single-particle spectral weight $A_{s=B,F}(\mathbf{p}, \omega)$ at $T_c$

Figure 10 shows  $A_{s=B,F}(\mathbf{p}, \omega)$  in a mass-imbalanced unitary Bose-Fermi mixture at  $T_c$ . In the Fermi SW (left panels), we find that effects of mass difference are different between the cases of  $m_B/m_F > 1$  and  $m_B/m_F < 1$ : Among the two sharp peaks (A and C) and the broad peak (B) in Fig. 10(a3), peak C, coming from the atom-molecule coupling, gradually disappears with increasing the ratio  $m_B/m_F > 1$  [decreasing from Fig. 10(a3) to Fig. 10(a1)]. When  $m_B/m_F$  decreases from unity, Figs. 10(a3)–10(a5) show that the broad peak (B), originating from the Fermi-Bose coupling, gradually disappears.

To understand these results, we plot in Fig. 11  $N_B^0 = \sum_p n_B(\xi_p^B)$  and  $N_{\text{CF}}^0 \equiv N_B - N_B^0$  [ $\sim N_{\text{CF}} = \sum_p f(\xi_p^{\text{CF}})$ ] in a unitary Bose-Fermi mixture at  $T_c$ . Noting that these quantities are directly related to the atom-molecule coupling and Fermi-Bose coupling, respectively [see Eq. (22)], we find from Fig. 11 that the former (latter) coupling phenomenon becomes dominant when  $R_m \rightarrow 1$  ( $R_m \rightarrow -1$ ). In addition, the momentum dependence of the Bose kinetic energy  $\xi_p^B$  becomes weak with increasing  $m_B$ , so that the broadening by the angular integration in the last term in the denominator of

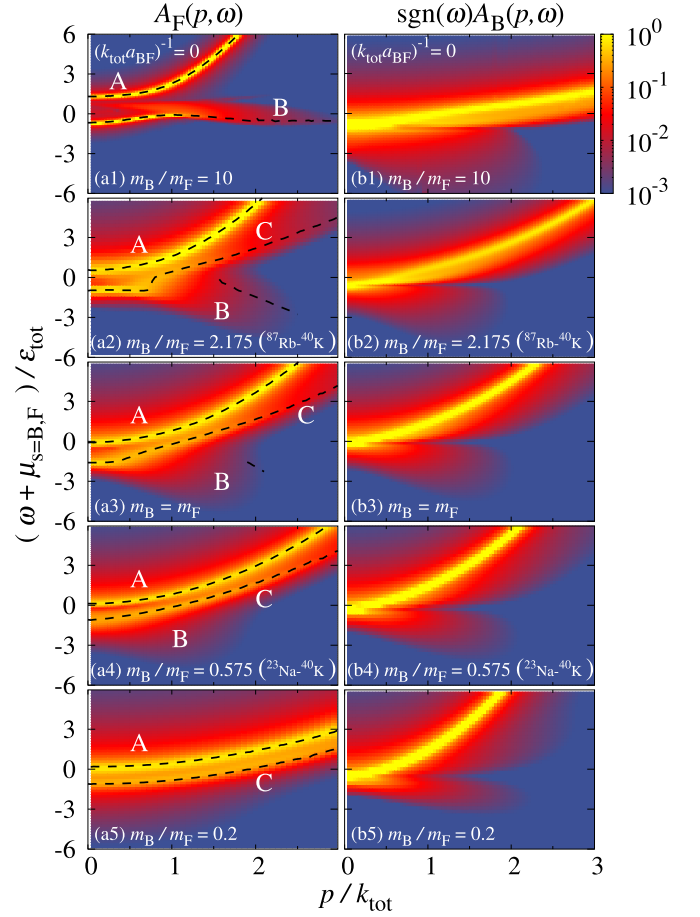


FIG. 10. Single-particle spectral weight in a unitary Bose-Fermi mixture with mass imbalance. We take  $T = T_c$  and  $N_B = N_F$ . The left and right panels show  $A_F(\mathbf{p}, \omega)$  and  $\text{sgn}(\omega)A_B(\mathbf{p}, \omega)$ , respectively. The second panels from the top (bottom) show the case of a  $^{87}\text{Rb}$ - $^{40}\text{K}$  ( $^{23}\text{Na}$ - $^{40}\text{K}$ ) mixture. For an eye guide, we plot the peak positions in the left figures (dashed lines).

Eq. (22) is suppressed. Because of this, the broad peak (B) in the mass-balanced case in Fig. 10(a3) gradually becomes sharp, as one moves from Fig. 10(a3) to Fig. 10(a1).

We next consider the Bose SW  $A_B(\mathbf{p}, \omega)$ . The right panels in Fig. 10 show that, with decreasing the ratio  $m_B/m_F$  [Figs. 10(b1)–10(b5)], the spectral intensity of the downward broad branch gradually becomes weak. Because this branch comes from the last term in the denominator of Eq. (25), the decrease of  $N_{\text{CF}}$  with decreasing  $m_B/m_F$  shown in Fig. 11 explains this behavior. We point out that this mechanism is the same as the suppression of the broad downward branch in the Fermi SW when  $m_B/m_F \ll 1$  (see the left panels in Fig. 10).

However, although the factor  $N_F^0$  is enhanced when  $m_B/m_F$  decreases (see Fig. 11), the coupling phenomenon coming from the second last term in the denominator of Eq. (25) is not clearly seen in Fig. 10(b5). This result is quite different from the case of Fermi SW, where the enhancement of  $N_B^0$  brings about the additional upward sharp peak line along the molecular dispersion, as seen in the left panels in Fig. 10. This difference originates from the fact that, while Bose excitations around  $\mathbf{q} = 0$  dominantly contribute to this coupling phenomenon in the latter case, Fermi atomic excitations around

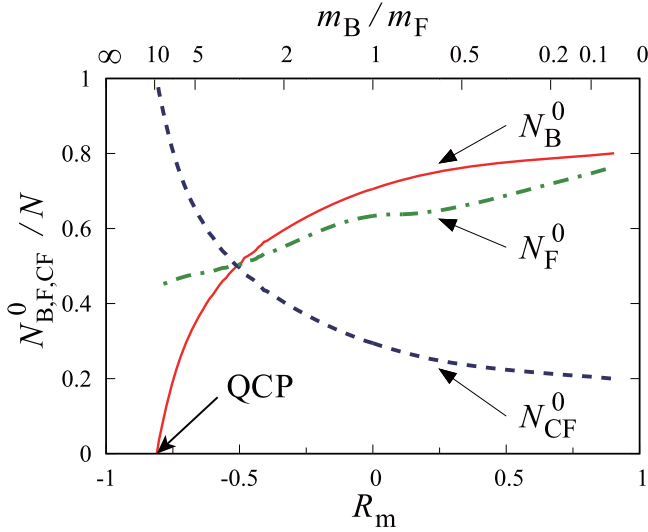


FIG. 11. The number  $N_B^0 = \sum_p n(\xi_p^B)$  of free Bose atoms, as well as the number  $N_{CF}^0 \equiv N_B - N_B^0$  of the Bose-Fermi molecules in a unitary Bose-Fermi mixture at  $T_c$ , as functions of mass imbalance parameter  $R_m$  in Eq. (31). We also plot the number  $N_F^0 = \sum_p f(\xi_p^F)$  of free Fermi atoms [52]. Since the direct evaluation of  $N_{CF} = \sum_p f(\xi_p^{CF})$  in Eq. (22) is difficult, we approximately use  $N_{CF}^0$  for  $N_{CF}$  in our discussions.

the Fermi surface are crucial for the former coupling phenomenon, which is reflected by the angular integration in the second to last term in the denominator of Eq. (25). As a result, while the coupling between a Fermi atom with momentum  $\mathbf{p}$  and a composite Fermi molecule having the same momentum leads to the appearance of a sharp spectral peak line along the molecular dispersion in  $A_F(\mathbf{p}, \omega)$ , the coupling of a Bose atom at momentum  $\mathbf{p}$  and composite Fermi molecules having various kinetic energies  $\xi_{k_{CF}-\mathbf{p}}^{CF}$  makes this coupling phenomenon obscure in  $A_B(\mathbf{p}, \omega)$ . Thus, as in the population-imbalanced case, the Fermi SW  $A_F(\mathbf{p}, \omega)$  is more suitable for the study of strong-coupling corrections to single-particle excitations in a mass-imbalanced Bose-Fermi mixture.

## V. EXAMPLES: $^{87}\text{Rb}$ - $^{40}\text{K}$ AND $^{23}\text{Na}$ - $^{40}\text{K}$ MIXTURES

### A. Outline and summary of main results in this section

In this section, we pick up  $^{87}\text{Rb}$ - $^{40}\text{K}$  and  $^{23}\text{Na}$ - $^{40}\text{K}$  mixtures, as typical examples of experimentally realized Bose-Fermi systems. Besides the Fermi SW  $A_F(\mathbf{p}, \omega)$  (which is not observable at the current experimental stage of cold atom physics), we also deal with the PES  $I_F(\mathbf{p}, \omega)$ , as an observable quantity involving information about single-particle excitations.

We find that, when  $N_B/N_F \gtrsim 1$ , the Fermi PES  $I_F(\mathbf{p}, \omega)$  exhibits a multiple-peak structure in both the unitary  $^{87}\text{Rb}$ - $^{40}\text{K}$  and  $^{23}\text{Na}$ - $^{40}\text{K}$  mixtures. Such an anomalous structure is absent when  $N_B/N_F \ll 1$ .

### B. Fermi single-particle spectral weight $A_F(\mathbf{p}, \omega)$

Figures 10(a2) and 10(a4) show the Fermi SW in the cases of  $^{87}\text{Rb}$ - $^{40}\text{K}$  and  $^{23}\text{Na}$ - $^{40}\text{K}$  mixtures, respectively. These

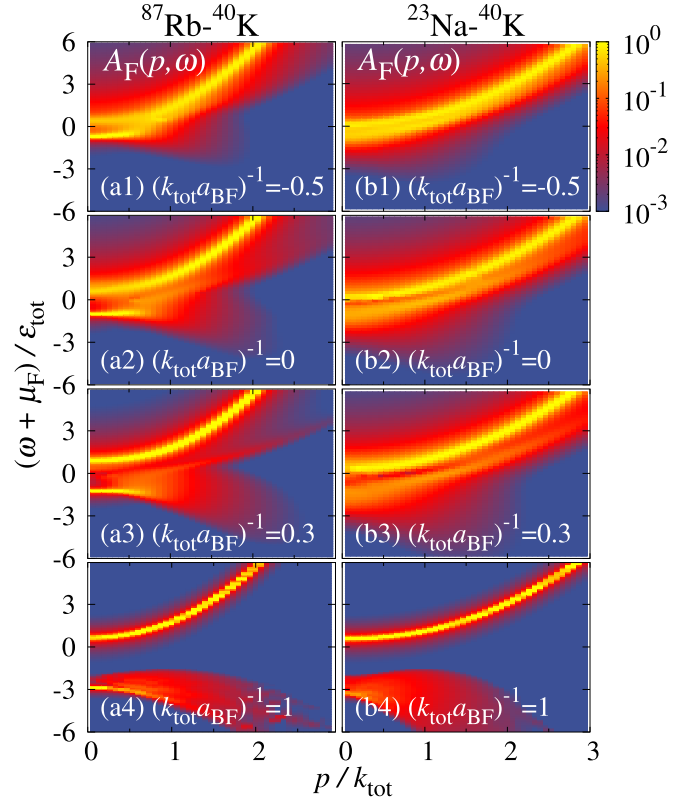


FIG. 12. Calculated Fermi SW  $A_F(\mathbf{p}, \omega)$  in a  $^{87}\text{Rb}$ - $^{40}\text{K}$  mixture (left panels), as well as a  $^{23}\text{Na}$ - $^{40}\text{K}$  mixture (right panels), at various interaction strengths ( $N_B = N_F$ ). We set  $T = T_c$  for the upper three cases. For the lowest case when  $(k_{\text{tot}} a_{\text{BF}})^{-1} = 1$ , because  $T_c$  is absent for  $(k_{\text{tot}} a_{\text{BF}}^c)^{-1} \geq 0.43$  in a  $^{87}\text{Rb}$ - $^{40}\text{K}$  mixture and for  $(k_{\text{tot}} a_{\text{BF}}^c)^{-1} \geq 0.7$  in a  $^{23}\text{Na}$ - $^{40}\text{K}$  mixture, we show the results in the normal state at  $T = 0.01T_c^0$  (which is the lowest temperature within our numerical calculation).

figures predict that the Fermi SW still exhibits the triple-peak structure in the  $^{87}\text{Rb}$ - $^{40}\text{K}$  case. Although the broad peak (B) is suppressed in a  $^{23}\text{Na}$ - $^{40}\text{K}$  mixture, we can still see the atom-molecule coupling in this mixture.

Figure 12 shows that these many-body coupling phenomena still remain to some extent, away from the unitary limit. In both the mixtures, the atom-molecule coupling is found to remain with *decreasing* the interaction strength (see the upper two panels in Fig. 12). This is simply due to the increase of  $N_B^0$  and the decrease of  $N_{CF}$  in the denominator in Eq. (22). As one *increases* the interaction strength (see the lowest two panels in Fig. 12), the Fermi-Bose coupling becomes important, reflecting the decrease of  $N_B^0$  and the increase of  $N_{CF}$ . In Figs. 12(a4) and 12(b4), only the Fermi-Bose coupling is seen.

### C. Fermi photoemission spectrum $I_F(\mathbf{p}, \omega)$

Figure 13 shows the Fermi PES  $I_F(\mathbf{p}, \omega)$  in a Bose-Fermi mixture, where the parameters in each panel are the same as those in the corresponding panel in Fig. 12. Comparing Figs. 12 and 13, one finds that, although the spectral structure seen in the positive-energy region of SW is suppressed by the Fermi distribution function in the PES [see Eq. (15)], it can still detect the downward broad spectral structure coming

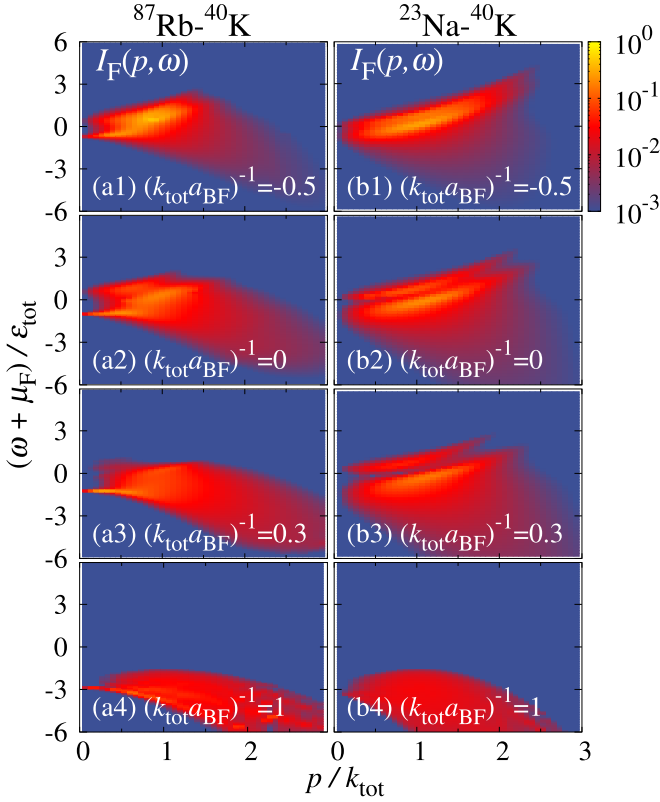


FIG. 13. Calculated Fermi PES  $I_F(p, \omega)$ . Left panels:  $^{87}\text{Rb}$ - $^{40}\text{K}$  mixture. Right panels:  $^{23}\text{Na}$ - $^{40}\text{K}$  mixture. The parameters are the same as those in Fig. 12. The spectral intensity is normalized by  $4\pi l_F^2 m$ . This normalization is also used in Figs. 14 and 15.

from the Fermi-Bose coupling associated with heteropairing fluctuations.

For the upward peak line along the molecular dispersion seen in the Fermi SW, since the thermal broadening of the Fermi distribution function  $f(\omega)$  around  $\omega = 0$  weakens the suppression of the spectral intensity in the positive-energy region in the Fermi PES, it gradually appears in the PES with increasing temperature, as shown in Fig. 14. Of course, this idea to observe the molecular branch is not always valid, especially for the very high-temperature region where Bose-Fermi molecules thermally dissociate into unpaired atoms. However, since the molecular binding energy is large in the strong-coupling regime, the temperature region where this idea works would be wide there.

Figure 15 shows effects of population imbalance on the Fermi PES  $I_F(p, \omega)$ . As expected from Fig. 3, the multiple peak structure gradually becomes obscure in  $I_F(p, \omega)$  with decreasing the ratio  $N_B/N_F$  from unity (see the upper two panels of Fig. 15). Noting that a real trapped Bose-Fermi mixture is always accompanied by local population imbalance [ $\rho_B(\mathbf{r}) \neq \rho_F(\mathbf{r})$ , where  $\rho_{s=F,B}(\mathbf{r})$  is the local density of the  $s$  component], one may interpret  $I_F(p, \omega)$  in Fig. 15 as the local PES at various spatial positions. Of course, in order to study detailed trap effects, we need to extend our theory to include effects of a harmonic potential. However, within this simple interpretation, one can still expect that the detailed spectral structure is smeared out after the spatial average of the

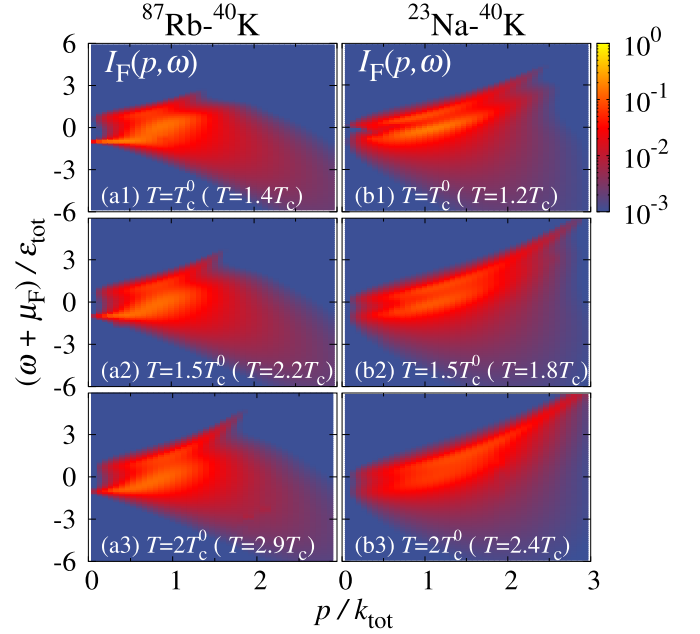


FIG. 14. Fermi PES  $I_F(p, \omega)$  in the unitary limit above  $T_c$ . We set  $N_B = N_F$ . Left panels:  $^{87}\text{Rb}$ - $^{40}\text{K}$  mixture ( $T_c = 0.695T_c^0$ ). Right panels:  $^{23}\text{Na}$ - $^{40}\text{K}$  mixture ( $T_c = 0.828T_c^0$ ). The results at  $T_c$  are shown in Figs. 13(a2) and 13(b2).

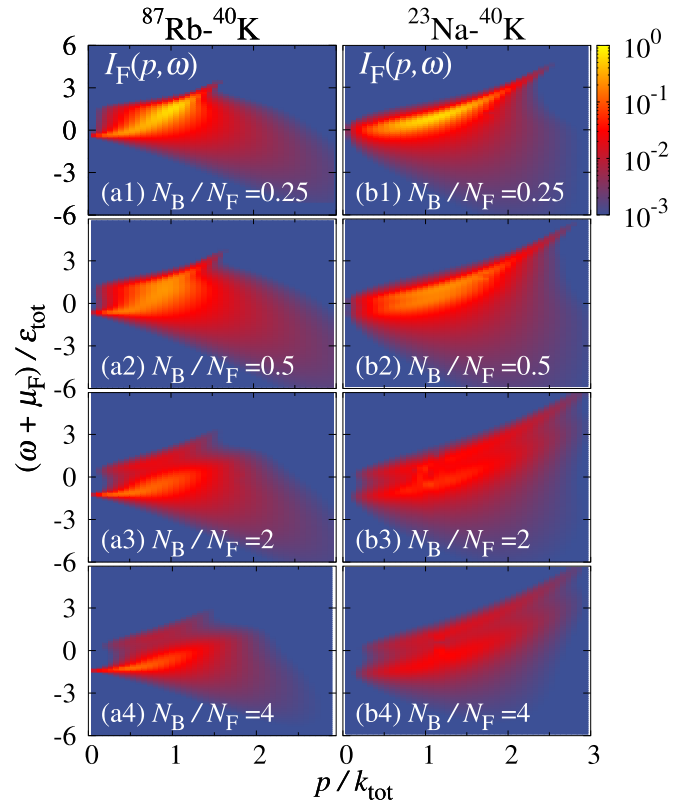


FIG. 15. Effects of population imbalance on the Fermi PES  $I_F(p, \omega)$  in a unitary Bose-Fermi mixture at  $T = 1.5T_c^0$ . Left panels:  $^{87}\text{Rb}$ - $^{40}\text{K}$  mixture. Right panels:  $^{23}\text{Na}$ - $^{40}\text{K}$  mixture. For the population-balanced results, see Figs. 13(a2) and 13(b2).

spectrum, when the dominant contribution to the spectrum comes from the spatial region where  $\rho_B(\mathbf{r}) \ll \rho_F(\mathbf{r})$  [see Figs. 15(a1) and 15(b1)]. To overcome this problem to some extent, one idea is to detect spectra, avoiding the spatial region where  $\rho_B(\mathbf{r}) \ll \rho_F(\mathbf{r})$ . For this purpose, the local photoemission-type experiment developed by the JILA group [41] would be useful. As an alternative way, a box trap [33–35] may also be promising, because an almost uniform gas is realized there.

## VI. SUMMARY

To summarize, we have discussed single-particle excitations and effects of mass and population imbalances in a Bose-Fermi mixture. Including heteropairing fluctuations associated with an attractive Bose-Fermi interaction within the framework of the improved  $T$ -matrix approximation developed by two of the authors, we calculated the single-particle spectral weight, as well as the photoemission spectrum, in the normal state above the BEC phase-transition temperature  $T_c$ .

In the mass- and population-balanced case ( $m_B = m_F$  and  $N_B = N_F$ ), it is known that strong heteropairing fluctuations cause couplings between atomic excitations and composite molecular excitations (atom-molecule coupling), as well as between Fermi atomic excitations and Bose atomic excitations (Fermi-Bose coupling). These many-body phenomena bring about two additional spectral peaks in the Fermi SW. Together with the ordinary spectral peak along the single-particle Fermi dispersion, the resulting Fermi SW exhibits a triple-peak structure.

In the presence of population imbalance, we showed that, when  $N_B/N_F \ll 1$ , both the atom-molecule and Fermi-Bose coupling phenomena become weak, so that the Fermi SW becomes close to that in a free Fermi gas. When  $N_B/N_F \gg 1$ , the former coupling continues to exist, leading to a double-peak structure in the Fermi SW. This difference comes from the fact that, while the atom-molecule coupling constant is dominated by the number of unpaired Bose atoms, the Fermi-Bose coupling constant is deeply related to the number  $N_{CF}$  of Bose-Fermi molecules [ $N_{CF} \leq \min(N_B, N_F)$ ]: Both coupling constants thus become small when  $N_B/N_F \ll 1$ . In contrast, the former coupling remains nonzero even when  $N_B/N_F \gg 1$ .

We have also examined how mass difference between a Fermi atom ( $m_F$ ) and a Bose atom ( $m_B$ ) modifies many-

body corrections to single-particle excitations. In both the limits  $m_B/m_F \ll 1$  and  $m_B/m_F \gg 1$ , we found that the Fermi SW exhibits not a triple-peak but a double-peak structure; however, their physical meanings are different. When  $m_B/m_F \ll 1$ , the atom-molecule coupling causes the second peak line in addition to the ordinary peak line along the free particle dispersion. In the opposite limit, the additional peak comes from the Fermi-Bose coupling. This is because the strengths of these couplings differently depend on the ratio  $m_B/m_F$ .

When one goes away from these limiting cases, the Fermi SW exhibits the triple-peak structure as in the mass-balanced case. We explicitly confirmed this in the cases of mass-imbalanced  $^{87}\text{Rb}$ - $^{40}\text{K}$  ( $m_B > m_F$ ) and  $^{23}\text{Na}$ - $^{40}\text{K}$  ( $m_B < m_F$ ) mixtures. We also pointed out that these many-body coupling phenomena may be observed by the photoemission-type experiment, by explicitly evaluating the photoemission spectra for these realistic examples.

In this paper, we have treated a uniform Bose-Fermi mixture, for simplicity. In a real trapped mixture in a harmonic potential, we expect that the Fermi and Bose atoms have different density profiles, leading to local population imbalance. Although this inhomogeneity effect has only partially been examined in this paper, by considering the population-imbalanced case, to fully understand strong-coupling properties of a trapped Bose-Fermi mixture, it would be necessary to explicitly treat the trapped geometry. Besides this, we have also ignored an interaction between Bose atoms, which would be crucial for the stability of this system [23,53]. These problems remain as our future challenges. Since the atom-molecule and Fermi-Bose couplings are characteristic many-body phenomena in a Bose-Fermi mixture with a heteropairing interaction, our results would contribute to further understanding of strong-coupling properties of this novel quantum many-body system.

## ACKNOWLEDGMENTS

We thank D. Kagamihara and R. Sato for discussions. This work was supported by the KiPAS project at Keio University. Y.O. was supported by a Grant-in-aid for Scientific Research from Ministry of Education, Culture, Sports, Science, and Technology and by Japan Society for the Promotion of Science (Grants No. JP18K11345, No. JP18H05406, and No. JP19K03689).

- 
- [1] I. Bloch, J. Dalibard, and W. Zwerger, *Rev. Mod. Phys.* **80**, 885 (2008).
  - [2] S. Giorgini, L. P. Pitaevskii, and S. Stringari, *Rev. Mod. Phys.* **80**, 1215 (2008).
  - [3] I. M. Georgescu, S. Ashhab, and F. Nori, *Rev. Mod. Phys.* **86**, 153 (2014).
  - [4] C. Gross and I. Bloch, *Science* **357**, 995 (2017).
  - [5] M. Greiner, O. Mandel, T. Esslinger, T. W. Hänsch, and I. Bloch, *Nature (London)* **415**, 39 (2002).
  - [6] C. A. Regal, M. Greiner, and D. S. Jin, *Phys. Rev. Lett.* **92**, 040403 (2004).
  - [7] M. W. Zwierlein, C. A. Stan, C. H. Schunck, S. M. F. Raupach, A. J. Kerman, and W. Ketterle, *Phys. Rev. Lett.* **92**, 120403 (2004).
  - [8] J. Kinast, S. L. Hemmer, M. E. Gehm, A. Turlapov, and J. E. Thomas, *Phys. Rev. Lett.* **92**, 150402 (2004).
  - [9] M. Bartenstein, A. Altmeyer, S. Riedl, S. Jochim, C. Chin, J. H. Denschlag, and R. Grimm, *Phys. Rev. Lett.* **92**, 203201 (2004).
  - [10] D. M. Eagles, *Phys. Rev.* **186**, 456 (1969).
  - [11] A. J. Leggett, in *Modern Trends in the Theory of Condensed Matter*, edited by A. Pekalski and J. Przystawa (Springer-Verlag, Berlin, 1980), p. 14.

- [12] C. A. R. Sá de Melo, M. Randeria, and J. R. Engelbrecht, *Phys. Rev. Lett.* **71**, 3202 (1993).
- [13] M. Randeria, in *Bose-Einstein Condensation*, edited by A. Griffin, D. W. Snoke, and S. Stringari (Cambridge University Press, New York, 1995).
- [14] G. C. Strinati, P. Pieri, G. Röpke, P. Schuck, and M. Urban, *Phys. Rep.* **738**, 1 (2018).
- [15] C. Chin, R. Grimm, P. Julienne, and E. Tiesinga, *Rev. Mod. Phys.* **82**, 1225 (2010).
- [16] S. Inouye, J. Goldwin, M. L. Olsen, C. Ticknor, J. L. Bohn, and D. S. Jin, *Phys. Rev. Lett.* **93**, 183201 (2004).
- [17] K.-K. Ni, S. Ospelkaus, M. H. G. de Miranda, A. Péer, B. Neyenhuis, J. J. Zirbel, S. Kotochigova, P. S. Julienne, D. S. Jin, and J. Ye, *Science* **322**, 231 (2008).
- [18] L. D. Macro, G. Valtolina, K. Matsuda, W. G. Tobias, J. P. Covey, and J. Ye, *Science* **363**, 853 (2019).
- [19] J. W. Park, C.-H. Wu, I. Santiago, T. G. Tiecke, S. Will, P. Ahmadi, and M. W. Zwierlein, *Phys. Rev. A* **85**, 051602(R) (2012).
- [20] C.-H. Wu, J. W. Park, P. Ahmadi, S. Will, and M. W. Zwierlein, *Phys. Rev. Lett.* **109**, 085301 (2012).
- [21] I. F. Barbut, M. Delehaye, S. Laurent, A. T. Grier, M. Pierce, B. S. Rem, F. Chevy, and C. Salmon, *Science* **345**, 1035 (2014).
- [22] H. Heiselberg, C. J. Pethick, H. Smith, and L. Viverit, *Phys. Rev. Lett.* **85**, 2418 (2000).
- [23] L. Viverit, C. J. Pethick, and H. Smith, *Phys. Rev. A* **61**, 053605 (2000).
- [24] T. Watanabe, T. Suzuki, and P. Schuck, *Phys. Rev. A* **78**, 033601 (2008).
- [25] E. Fratini and P. Pieri, *Phys. Rev. A* **81**, 051605(R) (2010).
- [26] D. Kharga, D. Inotani, R. Hanai, and Y. Ohashi, *J. Phys. Soc. Jpn.* **86**, 084301 (2017).
- [27] Z. Wu and G. M. Bruun, *Phys. Rev. Lett.* **117**, 245302 (2016).
- [28] K. Maeda, G. Baym, and T. Hatsuda, *Phys. Rev. Lett.* **103**, 085301 (2009).
- [29] S. Tsuchiya, R. Watanabe, and Y. Ohashi, *Phys. Rev. A* **80**, 033613 (2009).
- [30] R. Haussmann, M. Punk, and W. Zwerger, *Phys. Rev. A* **80**, 063612 (2009).
- [31] S. Tsuchiya, R. Watanabe, and Y. Ohashi, *Phys. Rev. A* **84**, 043647 (2011).
- [32] A. Perali, F. Palestini, P. Pieri, G. C. Strinati, J. T. Stewart, J. P. Gaebler, T. E. Drake, and D. S. Jin, *Phys. Rev. Lett.* **106**, 060402 (2011).
- [33] B. Mukherjee, Z. Yan, P. B. Patel, Z. Hadzibabic, T. Yefsah, J. Struck, and M. W. Zwierlein, *Phys. Rev. Lett.* **118**, 123401 (2017).
- [34] A. L. Gaunt, T. F. Schmidutz, I. Gotlibovych, R. P. Smith, and Z. Hadzibabic, *Phys. Rev. Lett.* **110**, 200406 (2013).
- [35] R. Lopes, C. Eigen, N. Navon, D. Clément, R. P. Smith, and Z. Hadzibabic, *Phys. Rev. Lett.* **119**, 190404 (2017).
- [36] G. E. Astrakharchik and L. P. Pitaevskii, *Phys. Rev. A* **70**, 013608 (2004).
- [37] M.-G. Hu, M. J. Van de Graaff, D. Kedar, J. P. Corson, E. A. Cornell, and D. S. Jin, *Phys. Rev. Lett.* **117**, 055301 (2016).
- [38] N. B. Jørgensen, L. Wacker, K. T. Skalmstang, M. M. Parish, J. Levinsen, R. S. Christensen, G. M. Bruun, and J. J. Arlt, *Phys. Rev. Lett.* **117**, 055302 (2016).
- [39] J. T. Stewart, J. P. Gaebler, and D. S. Jin, *Nature (London)* **454**, 744 (2008).
- [40] J. P. Gaebler, J. T. Stewart, T. E. Drake, D. S. Jin, A. Perali, P. Pieri, and G. C. Strinati, *Nat. Phys.* **6**, 569 (2010).
- [41] Y. Sagi, T. E. Drake, R. Paudel, R. Chapurin, and D. S. Jin, *Phys. Rev. Lett.* **114**, 075301 (2015).
- [42] P. Törmä, *Phys. Scr.* **91**, 043006 (2016).
- [43] M. Ota, H. Tajima, R. Hanai, D. Inotani, and Y. Ohashi, *Phys. Rev. A* **95**, 053623 (2017).
- [44] E. Fratini and P. Pieri, *Phys. Rev. A* **85**, 063618 (2012).
- [45] E. Fratini and P. Pieri, *Phys. Rev. A* **88**, 013627 (2013).
- [46] N. M. Hugenholtz and D. Pines, *Phys. Rev.* **116**, 489 (1959).
- [47] R. Haussmann, *Phys. Rev. B* **49**, 12975 (1994).
- [48] Although a two-body bound state vanishes at unitarity, medium effects give a bound state at this interaction strength, as will be explained later.
- [49] Reference [26] obtains Eq. (25) where the angular integration in the second to last term of the denominator is absent. This is because Ref. [26] deals with the more special case that  $\mu_F/\varepsilon_F \ll 1$ , that is,  $|\tilde{k}_F| = \sqrt{2m_F\mu_F} \sim 0$ . Because of this, the angular integration is not needed there.
- [50] S. P. Rath and R. Schmidt, *Phys. Rev. A* **88**, 053632 (2013).
- [51] J.-L. Song and F. Zhou, *Phys. Rev. A* **84**, 013601 (2011).
- [52] Although we impose the condition  $N_F = N_B$  in the population-balanced case, it does not necessarily give  $N_F^0 = N_B^0$ , as seen in Fig. 11. Thus, the number  $N_{CF}^0$  of Bose-Fermi molecules involves ambiguity, depending on whether it is defined as  $N_{CF}^0 = N_B - N_B^0$  or  $N_F - N_F^0$ . However, as shown in Fig. 11, because both  $N_B^0$  and  $N_F^0$  monotonically increase with increasing the mass imbalance parameter  $R_m$ , both the definitions qualitatively give the same  $R_m$  dependence of  $N_{CF}^0$ .
- [53] Z.-Q. Yu, S. Zhang, and H. Zhai, *Phys. Rev. A* **83**, 041603(R) (2011).